International Journal of Fluid Machinery and Systems
Vol. 3, No. 4, October-December 2010

DOI: 10.5293/IJFMS.2010.3.4.315
ISSN (Online): 1882-9554

Original Paper (Invited)

Compressible Simulation of Rotor-Stator Interaction in Pump-Turbines

Jianping Yan, Jiri Koutnik, Ulrich Seidel and Björn Hübner

Voith Hydro Holding GmbH & Co. KG
Alexanderstr. 11, 89522 Heidenheim, Germany
jianping.yan@voith.com, jiri.koutnik@voith.com
ulrich.seidel@voith.com, bjoern.huebner@voith.com

Abstract

This work investigates the influence of water compressibility on pressure pulsations induced by rotor-stator interaction (RSI) in hydraulic machinery, using the commercial CFD solver ANSYS-CFX. A pipe flow example with harmonic velocity excitation at the inlet plane is simulated using different grid densities and time step sizes. Results are compared with a validated code for hydraulic networks (SIMSEN). Subsequently, the solution procedure is applied to a simplified 2.5-dimensional pump-turbine configuration in prototype with different speeds of sound as well as in model scale with an adapted speed of sound. Pressure fluctuations are compared with numerical and experimental data based on prototype scale. The good agreement indicates that the scaling of acoustic effects with an adapted speed of sound works well. With respect to pressure fluctuation amplitudes along the centerline of runner channels, incompressible solutions exhibit a linear decrease while compressible solutions exhibit sinusoidal distributions with maximum values at half the channel length, coinciding with analytical solutions of one-dimensional acoustics. Furthermore, in compressible simulation the amplification of pressure fluctuations is observed from the inlet of stay vane channels to the spiral case wall. Finally, the procedure is applied to a three-dimensional pump configuration in model scale with adapted speed of sound. Normalized Pressure fluctuations are compared with results from prototype measurements. Compared to incompressible computations, compressible simulations provide similar pressure fluctuations in vaneless space, but pressure fluctuations in spiral case and penstock may be much higher.

Keywords: Compressible hydrodynamics, rotor-stator interaction, pump-turbine, unsteady CFD.

1. Introduction

Flow in hydraulic machinery is known to be unsteady. Pressure fluctuations induced by rotor-stator interaction (RSI) may be a major source of vibration and fatigue. Extensive literature is available on RSI and unsteady flow in hydro turbines (e.g. [1-6]). For many standard CFD applications, water compressibility does not play an important role and may be therefore neglected. However, typical RSI excitation frequencies of 50 to 200 Hz correspond to acoustic wavelengths of approximately 5 to 30 m, see wavelength-frequency dependence in Fig. 1. Hence, the acoustic wavelength in water may be in the range of prototype component dimensions. In such cases, acoustic resonance may occur, and acoustic effects may amplify pressure pulsations and may cause high amplitude structural vibrations. Therefore, it is important to study compressibility effects on pressure fluctuations induced by RSI in hydraulic machinery.

It is desired to perform hydraulic CFD in prototype scale. However, the Reynolds number is very high, and consequently neither compressible nor incompressible CFD simulations can resolve boundary layers properly. On the other hand, most hydraulic tests and measurements are based on model scale. Therefore, it is necessary and useful to perform CFD simulations of hydro turbines generally in model dimensions, but hydro-acoustic effects predicted in model scale should be valid for prototype machinery. As incompressible CFD does not consider the physics of acoustic phenomena, the transposition of computed pressure pulsations from the computational model to prototype conditions may be not physical for some parts of the turbine. Acoustic effects in hydraulic model scale tests are also not transposable to prototype size machinery. In contrast, compressible CFD simulations in model scale with adapted speed of sound (to scale acoustic effects) may be a good solution. The present study can be considered as a numerical experiment to investigate this topic.

Accepted for publication November 29, 2010: Paper number O10039S
Corresponding author: Jianping Yan, Dr.-Ing., jianping.yan@voith.com

This manuscript was presented at the 25th IAHR Symposium on Hydraulic Machinery and Systems, September 20-24, 2010, Politechnica University of Timisoara, Romania .

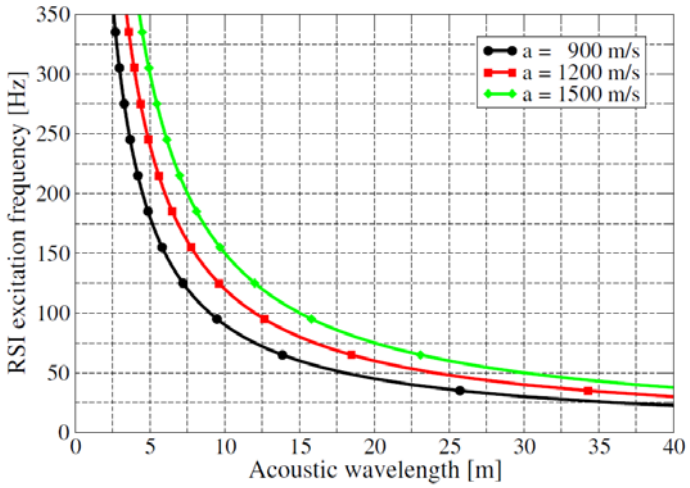

Fig. 1 Acoustic wavelength depending on frequency for different speeds of sound

Hydraulic compressibility effects can be properly taken into account by compressible CFD based on Navier-Stokes equations for weakly compressible fluids, incorporating the equation of state for water

$$\rho = \rho_0 + (p - p_0)/a_0^2 \quad , \tag{1}$$

where the subscript 0 denotes a reference quantity, ρ the density, and p the pressure. The speed of sound a_0 is assumed to be constant. Therefore, the influence of compressibility effects can be investigated using different speeds of sound such as 900 m/s, 1100 m/s, and 1300 m/s which reveal phenomena of interest in hydraulic machinery.

The current paper demonstrates the ability of compressible CFD to predict acoustic effects in hydraulic machinery and to provide a better understanding of the influence of water compressibility on pressure fluctuations induced by RSI. At first, pipe flow with a harmonic velocity excitation is simulated using different grid densities and time step sizes. The computed results are compared with those predicted by a validated code for hydraulic networks (SIMSEN). Subsequently, the calibrated numerical method is applied to a simplified 2.5-dimensional pump-turbine configuration in prototype as well as in model scale with an adapted speed of sound. Normalized pressure fluctuations are compared to numerical and experimental results of a prototype. Finally, a fully three-dimensional configuration of a pump in model scale is investigated. The numerical results are compared with normalized experimental data.

2. Evaluation of Compressible CFD for Hydraulic Applications

As illustrated in Fig. 2, a pipe flow configuration with a length of L = 10 m and a diameter of D = 0.1 m is regarded. Using the validated software SIMSEN [7], pipe flow dynamics is investigated for harmonic velocity fluctuations at the inlet. A grid width of $\Delta z = 0.02$ m and a time step size of $\Delta t = 5 \cdot 10^{-5}$ s apply for computing the reference solution which is used to evaluate results of compressible CFD simulations.

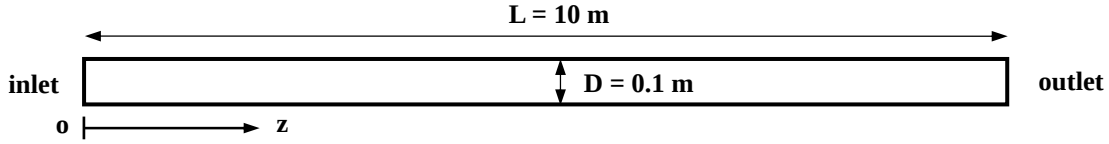

Fig. 2 Pipe flow configuration

Block structured hexahedral meshes with a uniform grid in axial direction apply for compressible CFD simulation with ANSYS-CFX. Two different discretizations are used, namely, a fine resolution ($\Delta z = 0.02$ m and $\Delta t = 5 \cdot 10^{-5}$ s) matching with the SIMSEN discretization and a coarser resolution ($\Delta z = 0.05$ m and $\Delta t = 2.5 \cdot 10^{-4}$ s) comparable to the discretization of runner channels in the simplified pump-turbine configuration in prototype scale. At the inlet plane, the flow is assumed to be fully turbulent using the mean velocity profile

$$\overline{w} = w_0 \left(\frac{r_0 - r}{r_0} \right)^{1/7} , \tag{2}$$

where $r_0 = 0.05$ m is the radius of the pipe and $w_0 = 30$ m/s the mean velocity at center position. The harmonically fluctuating part of the inlet velocity

$$\Delta w = 0.1 \cdot \overline{w} \cdot 0.5 \cdot \left(1 - \cos(2\pi \cdot f \cdot t)\right) \tag{3}$$

is added to the mean velocity profile $\overline{w}$ given in Eq. (2). In Eq. (3), $f = 60$ Hz is the excitation frequency and t the physical time.

The speed of sound is assumed to be 1000 m/s, and the density of water is defined by Eq. (1). The high resolution advection scheme of CFX, the second order backward Euler method for time integration, and the k-ε turbulence model with scalable wall functions are used. For inlet and outlet boundary conditions, the option "reflective" is selected in the acoustic reflectivity. As convergence criterion the RMS residual target is set to $5 \cdot 10^{-6}$ for velocity components and pressure. For unsteady simulations, the steady state solution is taken as initial condition, and time-dependent velocity distributions are specified at the inlet plane. The computed physical time is 0.2 s corresponding to 10 wave propagation periods in the pipe. Monitor points are placed on the centreline of the pipe to evaluate the results.

Figure 3 shows time histories of pressures at $z = 0$ m (solid lines) and $z = 4$ m (dashed lines) on the centerline of the pipe predicted by CFX and SIMSEN. The black lines represent the fine resolution, the blue lines the coarse one, while the red lines stand for SIMSEN. Although CFX results are based on 3-dimensional unsteady Reynolds-Averaged Navier-Stokes equations (URANS) and SIMSEN solutions based on one-dimensional hydro-acoustic analyses, they agree with each other fairly well. Furthermore, pressure difference between the fine and coarse resolutions is quite small. Therefore, the present hydraulic compressible CFD is proven to give realistic results and may be applied to prediction of dynamic pressure pulsations in complex hydraulic machinery.

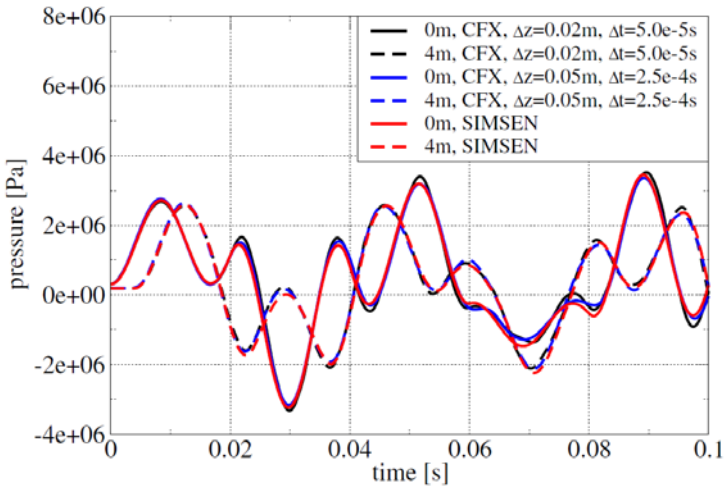

Fig. 3 Time histories of pressure predicted by CFX with different discretizations and by SIMSEN

3. Compressible Simulation of RSI in a Simplified Pump-Turbine Configuration

3.1 Modeling and Numerical Setup

The computational domain of regarded pump-turbine with a specific speed of n_q=50 consists of a spiral case, a tandem cascade with 20 stay vanes and wicket gates, a runner with 9 blades, and a draft tube, considering the influence of non-uniform inflow from the spiral case. The regarded turbine mode operating point is 70% wicket gate opening close to optimum. Since this study is focused on the influence of compressibility effects on pressure pulsations, the original configuration is reduced to a simplified 2.5-dimensional model, see Fig. 4, minimizing the computational effort. The third dimension is not of a constant thickness but reflects the varying cross-sectional area.

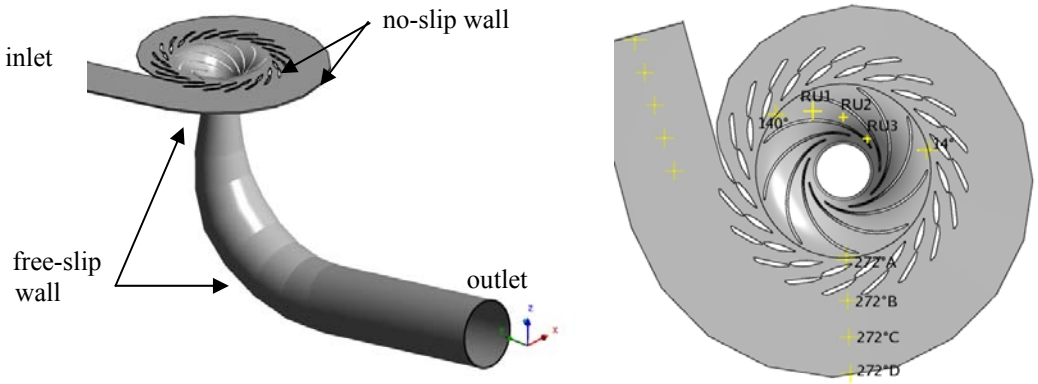

(a) (b)

Fig. 4 Configuration of the 2.5-dimensional model (a) and locations of monitor points (b)

Using different speeds of sound, this prototype configuration has been used to investigate the effect of water compressibility in previous work [1]. For simulations at model scale, the structured hexahedral mesh in prototype size is scaled to model dimensions. At the inlet plane, the mass flow rate with normal flow direction is specified, and at the outlet plane, an opening condition is applied. All surfaces of turbine components which are in contact to the water passage are defined as no-slip walls, while the remaining surfaces which reduce the third dimension to a small distance are defined as free-slip walls, see Fig. 4 (a). Between opposed free-slip walls, only two elements are located.

The time step size is selected such that one runner revolution is divided into 400 time steps corresponding to an angular change of 0.9 degree and being sufficient to resolve dynamic effects of interest. For all computations, 10 revolutions are carried out. The last revolution is used to plot time histories of pressure fluctuations, while the last 6 revolutions are used to perform Fourier transformations of time domain results.

The high resolution advection scheme of CFX, the second order backward Euler method for time integration, and the k-ε turbulence model with scalable wall functions are used. The RMS residual target is set to 10^{-5} for velocity components and pressure to ensure converged solutions. Between rotating and stationary components, circumferential averaging is used for steady state calculations and a transient rotor-stator interface for unsteady simulations. The steady state solution is taken as initial condition for unsteady simulations. Since non-reflecting acoustic boundary conditions implemented in CFX do not work properly for high pressure fluctuations, a special technique is introduced by means of user subroutines to remedy reflections of acoustical waves at inlet and outlet boundaries and to improve the convergence behavior.

Monitor points are defined to evaluate the results. RU1, RU2, and RU3 are placed on the centerline of a runner channel, while monitor point 14° is located in vaneless space in the stationary domain close to the rotor-stator interface, see Fig. 4 (b).

In order to transpose acoustic effects predicted in model scale simulations to prototype conditions, the simplified pump-turbine configuration in model scale is simulated with an adapted sonic speed of 348 m/s which corresponds to a value of 1100 m/s in prototype scale. To compare dynamic effects in different scales, frequencies are divided by the rotational frequency of the runner f_r and pressure fluctuations are normalized according to

$$P^* = (p - \bar{p})/(0.5\rho_0 R_0^2 \omega^2) \quad , \tag{4}$$

where $\bar{p}$ denotes the time averaged pressure, R_0 the external runner radius, and ω the angular frequency of the runner speed.

3.2 Results

Time histories of pressure fluctuations measured in the prototype (experimental) are compared with numerical results at monitor point 14° in vaneless space in the stationary frame of reference, see Fig. 5 (a). In the prototype, the dynamic pressure in vaneless space was measured with a flush mounted pressure sensor of the type PCB 121A31/AB. The black line represents the compressible simulation in model scale with adapted speed of sound, the red line the compressible simulation in prototype scale, and the blue line the incompressible simulation in prototype scale. Both experimental and numerical results are clearly periodical and stable. The agreement between measurement and all simulations is quite good. However, the amplitude of the second harmonic cannot be captured accurately by the incompressible simulation, but is well predicted by compressible simulations, see the small picture in Fig. 5 (a) with enlarged time histories of normalized pressure fluctuations. Pressure fluctuations of the different compressible simulations are very similar. Deviations may be explained by different resolutions of boundary layer effects in prototype and model scale.

Frequency spectra of pressure fluctuations from numerical results are given in Fig. 5 (b). The peaks correspond to the blade passing frequency $f_{BPF} = 9\, f_r$ (frequency of rotation times number of runner blades) and its higher harmonics. For the first harmonic ($f/f_r = 9$), pressure amplitudes are nearly equal for all types of simulation. The most significant difference between compressible and incompressible simulations arises at the second harmonic of the blade passing frequency ($f/f_r = 18$), where compressible simulations exhibit higher amplitudes than incompressible simulations. Comparing compressible simulations in model and prototype scale, pressure fluctuation amplitudes are almost equal for all harmonics.

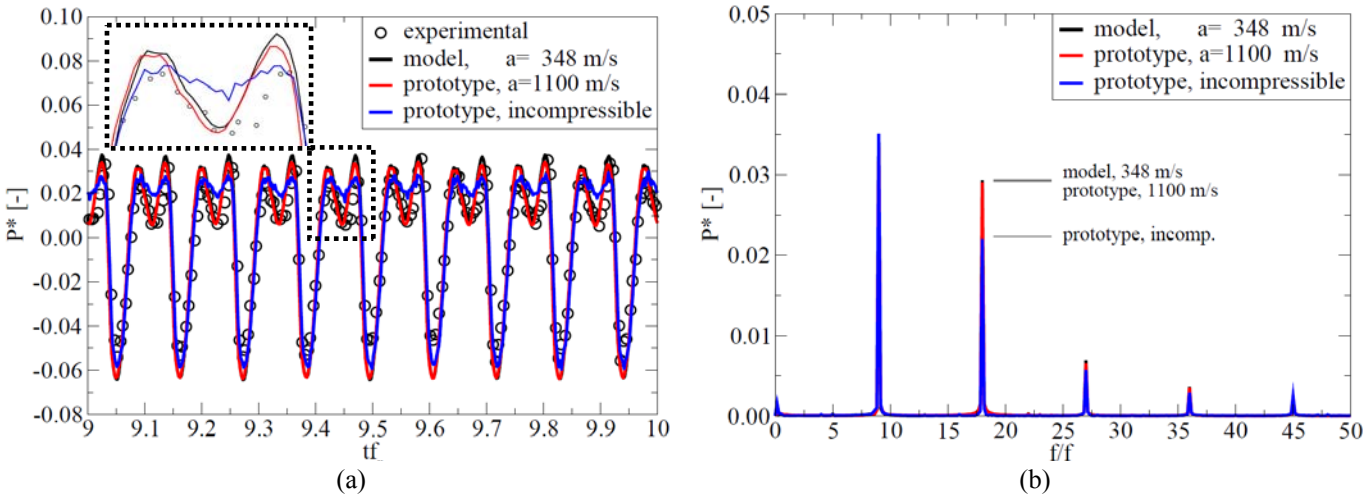

(a) (b)

Fig. 5 Comparison of pressure fluctuations in time domain (a) and frequency domain (b) at monitor point 14° (vaneless space − stationary frame of reference)

Looking at time histories and corresponding frequency spectra of normalized pressure fluctuations at monitor points RU1, RU2 and RU3 inside of a runner channel, two dominant frequencies can be detected, see Fig. 6. On the one hand the frequency of runner rotation f_r and on the other hand the gate passing frequency $f_{GPF} = 20\, f_r$ (frequency of rotation times number of wicket gates). The amplitude at f_r which is caused by the spiral case is comparable to the amplitude at f_{GPF} and should be considered for fatigue life evaluations, too. At f_{GPF}, pressure fluctuations of compressible simulations exceed those of the incompressible simulation clearly. In contrast, pressure fluctuations of compressible simulations in model scale with adapted speed of sound and in prototype scale are almost equal.

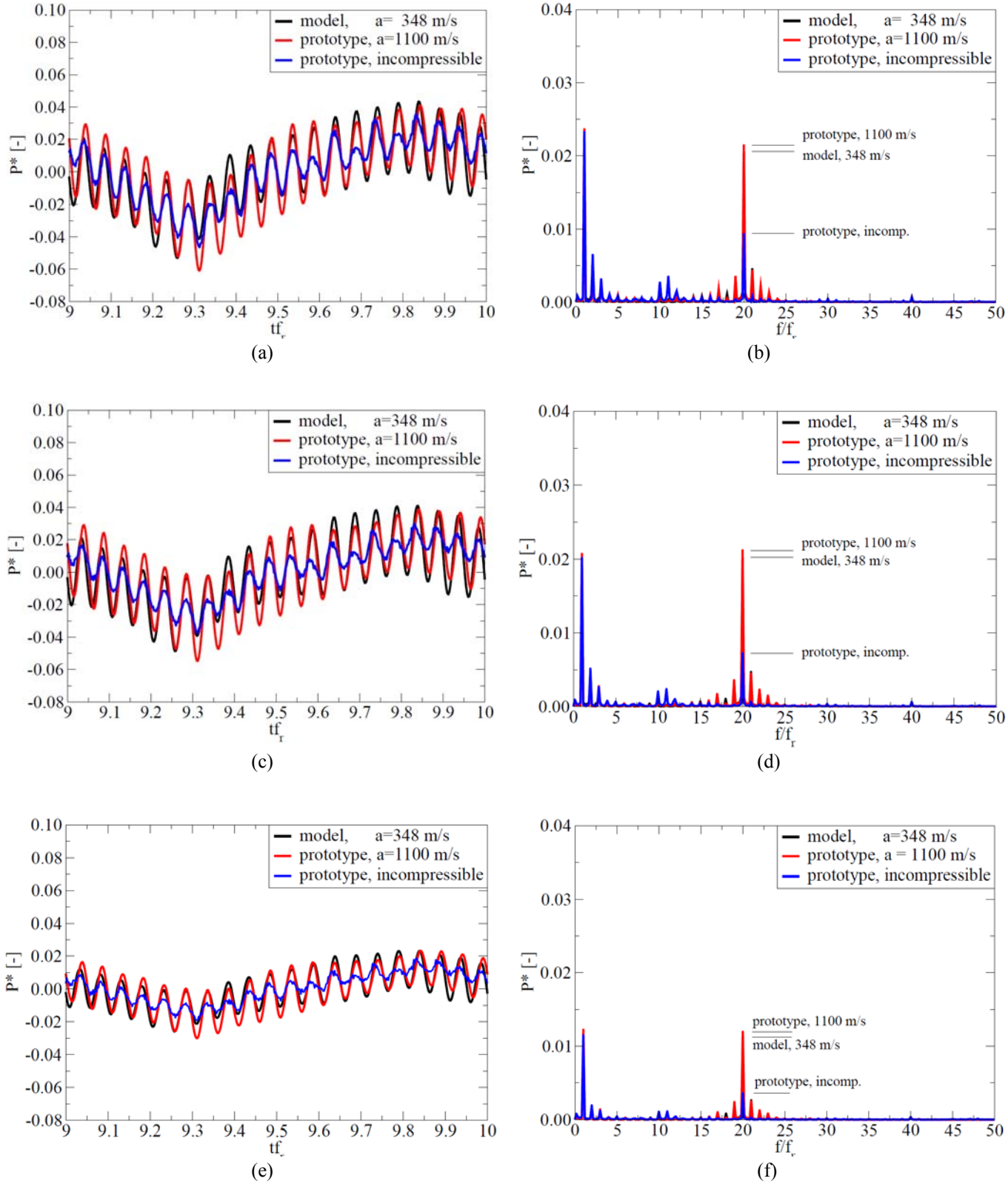

Fig. 6 Comparison of pressure fluctuations in time domain and frequency domain at monitor points RU1 (a, b), RU2 (c, d) and RU3 (e, f)

For a better understanding of the influence of water compressibility on pressure fluctuations inside of runner channels, pressure amplitudes from the different simulations belonging to the gate passing frequency f_{GPF} are compared in Fig. 7 (a) at monitor points RU1, RU2, and RU3. In addition to the sonic speed of $a_0 = 1100$ m/s, compressible results in prototype scale are given also for $a_0 = 900$ m/s and $a_0 = 1300$ m/s. Comparing pressure fluctuation amplitudes of the model scale simulation with adapted sonic speed of $a_0 = 348$ m/s with corresponding prototype scale results for $a_0 = 1100$ m/s, good agreement is observed with slightly smaller amplitudes in model scale simulations.

Considering that the distance between monitor points RU2 and RU3 is larger than the distance between RU1 and RU2, pressure amplitudes of the incompressible simulation decrease linearly along centerlines of runner channels. In contrast, pressure amplitudes of compressible simulations exhibit sinusoidal distributions. This behavior coincides with a simplified analytical approach of one-dimensional acoustics, shown in Fig. 7 (b), where L is the length of a runner channel and $\lambda = a_0/f$ the acoustic wavelength. The linear pressure characteristics ($L/\lambda << 1/4$) is valid for incompressible fluids, and with increasing compressibility (decreasing sonic speed and wavelength) the sinusoidal pressure characteristic becomes more evident, up to a value of $L/\lambda = 1/2$ where resonance occurs. In prototype scale, acoustic resonance is observed at a sonic speed of approximately 900 m/s.

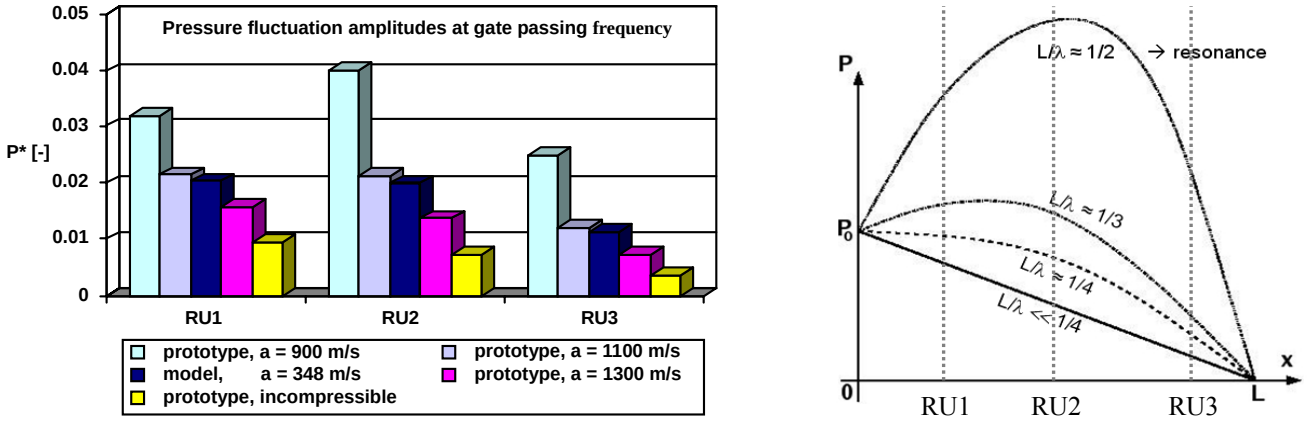

(a) (b)

Fig. 7 Comparison of pressure fluctuation amplitudes at gate passing frequency for monitor points on runner channel centerline (a) and simplified analytical approach considering 1-dimensional acoustics (b)

To study the pressure evolution in the radial direction, the pressure fluctuations and frequency spectra at monitor points Stat272°A, B, C and D are presented in Fig. 8. They are taken from the compressible simulation with a speed of sound of 900 m/s in prototype. Stat°272A is located in vaneless space in the stationary domain close to the rotor-stator interface, Stat270°B at the inlet of stay vane channels and Stat272°D close to the spiral case wall. Stat272°C is the midpoint of Stat272°B and Stat272°D. The large pressure fluctuations forming in the rotor-stator zone decrease very fast in the upstream direction, except the 2nd harmonic of blade passing frequency (f/f_r=18). The amplitude of pressure fluctuations of f/f_r=18 is amplified from the inlet of stay vane channels to the spiral case wall, as seen in the small picture in Fig. 8 (b), where the red line stands for Stat272°B, the green for Stat272°C and the blue for Stat272°D. This phenomenon coincides with harmonic response analyses of an acoustic fluid.

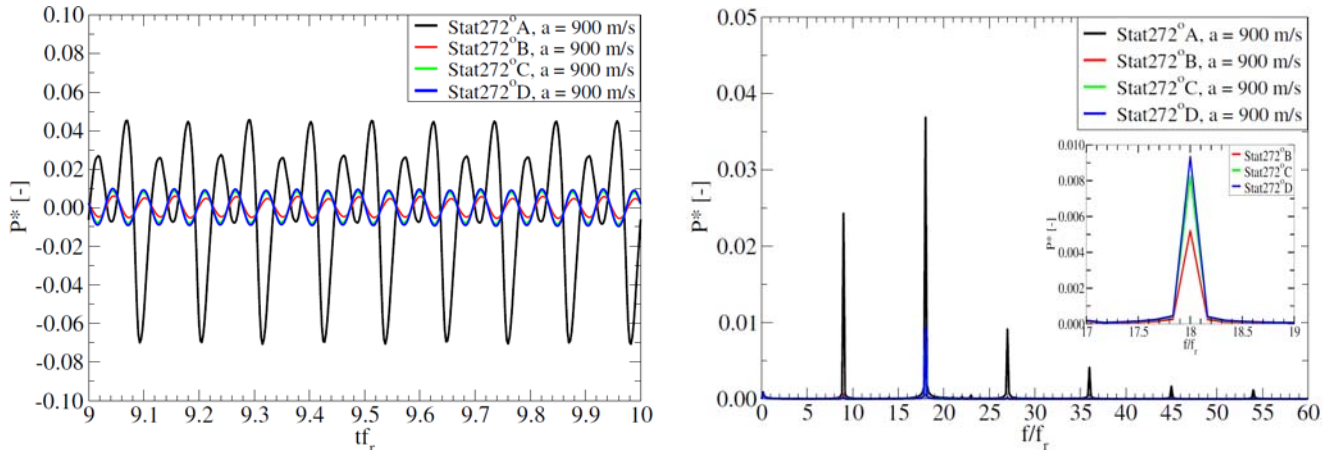

(a) (b)

Fig. 8 Pressure fluctuations (a) and frequency spectra (b) of compressible simulation with a speed of sound of 900 m/s at monitor points Stat272°, A, B, C and D at a radial line across distributor and spiral case

Figure 9 shows dynamic pressure contours of the compressible simulation with a speed of sound of 900 m/s and the incompressible simulation. The acoustic mode with 2 diametrical node lines (k=-2) is clearly evidenced by the compressible simulation and the amplification of pressure fluctuation amplitudes is visually confirmed too, see Fig. 9 (a).

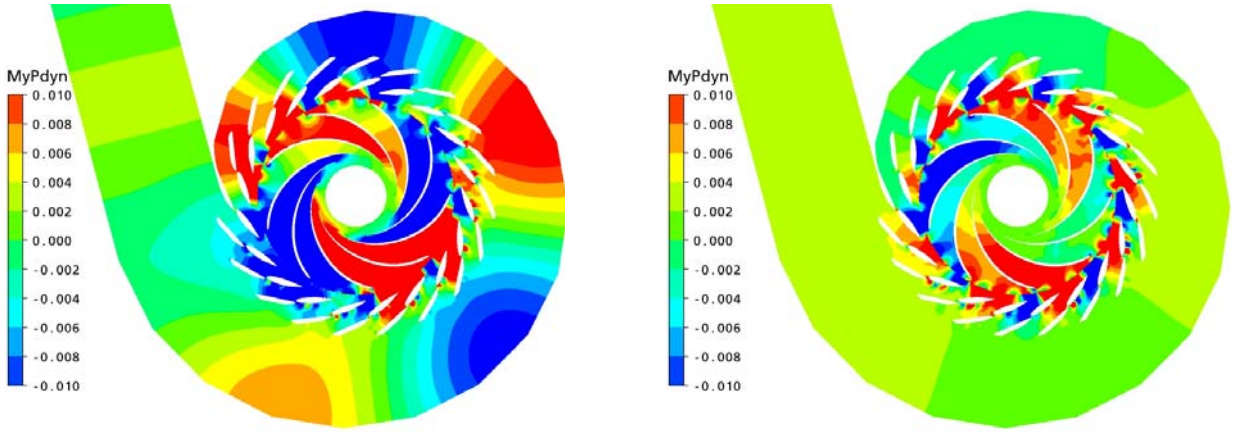

(a) (b)

Fig. 9 Dynamic pressure contours: (a) compressible simulation with a speed of sound of 900m/s and (b) incompressible simulation

Summarizing the results of the simplified pump-turbine example, it can be concluded that compressibility effects of water may strongly influence pressure fluctuations in hydraulic turbines and pumps, especially in the frequency range of rotor-stator interaction. Moreover, compressible CFD simulations may be carried out in model scale if acoustic effects are scaled properly by using an adapted speed of sound.

4. Compressible Simulation of RSI in a 3-Dimensional Pump Configuration in Model Scale

The computational model of the pump (specific speed of n_q=27) investigated in this work is based on the configuration of a hydraulic model scale test. The computational domain consists of a draft tube cone, an impeller with 7 blades, a stay ring with 12 identical stay vanes, a spiral case, and a connection pipe to the penstock, see Fig. 10 (a). The computational domain is discretized with a completely structured hexahedral mesh of approximately 5 million elements. While the spiral case grid was generated using the ICEM Hexa software, the remaining components were meshed by an in-house automated meshing procedure which is also applied to the standard hydraulic design applications. A detailed grid view is given in Fig. 10 (b).

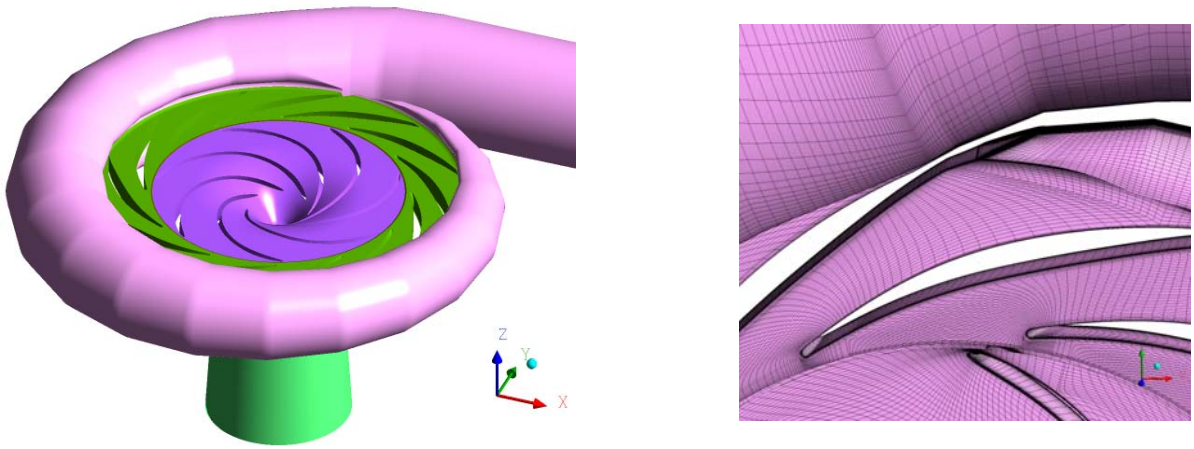

(a) (b)

Fig. 10 Full view of configuration (a) and detailed grid view (b)

At normal pump operation, the computational model is analyzed by means of compressible and incompressible simulations. For compressible simulations, an adapted sonic speed of 523 m/s is used in order to scale acoustic effects properly. The time step size is selected such that one runner revolution is divided into 360 time steps corresponding to an angular change of 1 degree. At the inlet plane of the draft tube cone, the mass flow rate with normal flow direction is specified, and at the outlet plane of the spiral case extension, an opening condition is used. No-slip wall conditions are defined at all surfaces of turbine components

which are in contact to the water passage. The high resolution advection scheme of CFX, the second order backward Euler method for time integration, and the SST turbulence model are used. The RMS residual target is set to $2 \cdot 10^{-5}$ for velocity components and pressure to ensure converged solutions.

Dynamic pressures contours from compressible and incompressible CFD simulations are compared in Fig. 11 (a) and (b), where the "+" denotes the position of the monitor point SCdyn in the spiral case extension. At the corresponding prototype position, dynamic pressure data is available from site measurements using a flush mounted pressure sensor of the type PCB S111A26. In both cases, a rotating pressure field with 2 diametrical node lines (k = 2) which is induced by RSI is visible inside of impeller channels and in the stay ring area. However, in contrast to the incompressible solution in Fig. 11 (b), the compressible solution in Fig. 11 (a) also predicts the k=2 pressure field in the spiral case, and pressure fluctuations in the spiral case extension (monitor point SCdyn) are still very strong.

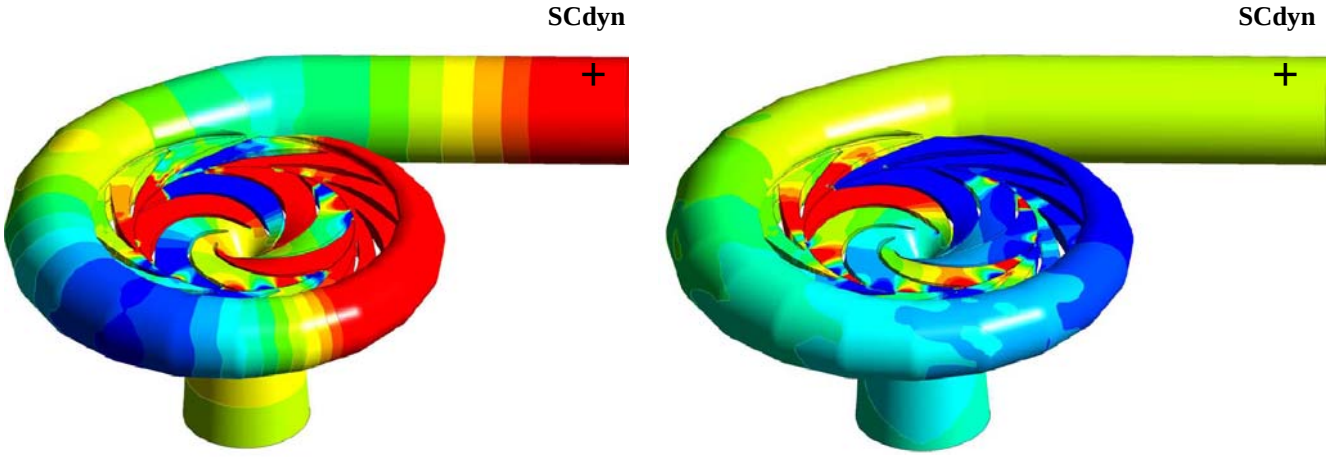

(a) (b)

Fig. 11 Pump configuration in model scale with dynamic pressure contours: compressible simulation with adapted sonic speed of 523 m/s (a) and incompressible simulation (b)

Time histories of pressure fluctuations from numerical simulations at monitor point SCdyn are compared to results from prototype measurements (experimental) using normalized pressure values according to Eq. (4), see Fig. 12 (a). The incompressible simulation cannot predict at all the measured pressure fluctuations at monitor point SCdyn. In contrast, the compressible solution predicts quite well the amplitude of the second harmonic of the blade passing frequency which is the major pressure amplitude measured in the prototype, but it overestimates the amplitude of the first harmonic considerably. Here, further investigations are necessary to clarify this result.

In contrast, efficiency fluctuations and time-averaged efficiency values of compressible simulations agree quite well with the respective values of incompressible simulations, see time histories of efficiency fluctuations normalized with the time-averaged efficiency of the incompressible simulation in Fig. 12 (b). Hence, compressibility effects have only minor influence on the efficiency of hydraulic turbines and pumps.

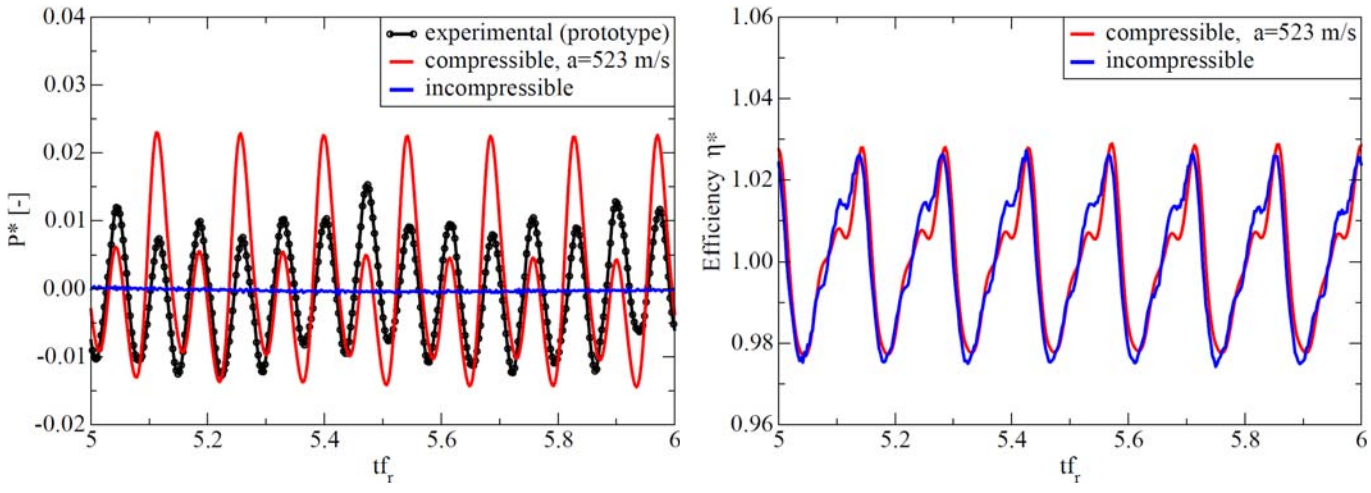

(a) (b)

Fig. 12 Time histories of computed pressure fluctuations at monitor point SCdyn (a) and efficiency fluctuations (b)

5. Conclusion

By means of a pipe flow example with harmonically varying inlet velocity, compressible CFD simulations with ANSYS-CFX are compared to the validated one-dimensional code SIMSEN. The solution procedure is proven to give realistic results and may be used to predict pressure pulsations in hydraulic machinery. Compressible CFX simulations of rotor-stator interaction (RSI) are performed for a simplified pump-turbine and a complete pump model demonstrating that compressibility effects of water may strongly influence pressure fluctuations in hydraulic turbines and pumps. Incompressible simulations of RSI may predict pressure fluctuations in vaneless space, but they may strongly underestimate pressure fluctuations in spiral case or runner channels if acoustic effects (e.g. resonance) are of great importance. In contrast, compressible CFD simulations of hydraulic turbines account for acoustic effects and may be performed in model scale, if acoustic effects are scaled properly by using an adapted speed of sound.

Nomenclature

a_0	Speed of sound [m/s]	t	Time [s]
f	Frequency [Hz]	w, w_0	Velocity and reference velocity component [m/s]
p, p_0	Pressure and reference pressure [Pa]	ω	Angular frequency of runner speed [rad/s]
r, R	Radius [m]	ρ, ρ_0	Density and reference density [kg/m^3]

References

[1] Yan, J., Koutnik, J., Seidel, U. and Hübner, B., 2009, "Compressible Simulation of Rotor-Stator Interaction in a Pump-Turbine," 3rd IAHR International Meeting of the Workgroup on Cavitation and Dynamic problems in Hydraulic Machinery and System, Brno.

[2] Gagnon, J.M. and Deschenes, C., 2008, "Numerical Simulation of a Rotor-Stator Unsteady Interaction in a Propeller Turbine," 24th Symposium on Hydraulic Machinery and Systems, Foz Do Iguassu.

[3] Guedes, A., Kueny, J.L., Ciaocan, G.D. and Avellan, F., 2002, "Unsteady Rotor-Stator Analysis of a Hydraulic Pump-Turbine: CFD and Experimental Approach," 21st Symposium on Hydraulic Machinery and Systems, Lausanne.

[4] Flemming, F., Aschenbrenner, T., Jung, A. and Fisher, R.K., 2008, "Optimization of an Adjustable Speed Pump-Turbine using Unsteady Flow Simulations," HydroVision 2008, Sacramento, CA, USA.

[5] Nennemann, B., Vu, T.C. and Farhat, M., 2006, "CFD Prediction of Unsteady Wicket Gate-Runner Interaction in Francis Turbines: A New Standard Hydraulic Design Procedure," 23rd Symposium on Hydraulic Machinery and Systems, Yokohama.

[6] Zobeiri, A., Kueny, J., Farhat, M. and Avellan, F., 2006, "Pump-Turbine Rotor-Stator Interactions in Generating Mode: Pressure Fluctuation in Distributor Channel," 23rd Symposium on Hydraulic Machinery and Systems, Yokohama.

[7] Nicolet, C., Avellan, F., Allenbach, P., Sapin, A. and Simond, J., 2002, "New Tools for the Simulation of Transient Phenomena in Francis Turbine Power Plants," 21st Symposium on Hydraulic Machinery and Systems, Lausanne.